A Physical Model for MR-DTI Based Connectivity Map Computation

Erdem Yörük[1], Burak Acar[1], and Roland Bammer[2]

[1] Department of Electrical-Electronic Engineering, Bogazici University, TURKEY,
erdem.yoruk@boun.edu.tr,
[2] Department of Radiology, Stanford University, USA,

Abstract. In this study we address the problem of extracting a robust connectivity metric for brain white matter. We defined the connectivity problem as an energy minimization task, by associating the DT-field to a physical system composed of nodes and springs, with their constants defined as a function of local structure. Using a variational approach we formulated a fast and stable map evolution, which utilizes an anisotropic kernel smoothing scheme equivalent to a diffusion PDE. The proposed method provides connectivity maps that correlate with normal anatomy on real patient data.

1 Introduction

Magnetic Resonance Diffusion Tensor Imaging (MR-DTI) is a recent technique that provides information about the geometry of fiberous structures, such as the fibers in the human brain, in vivo. MR-DTI is based on measuring the diffusion of water molecules. The diffusion process is approximated by a second order tensor. It was shown that the principal eigenvector of this tensor is correlated with the underlying fiberous structures' orientation in places where there are such structures. So, MR-DTI has been accepted as a promising tool to get information about the connections in human brain, esp. for several diseases. Despite its promise, DTI has its drawbacks: Low order approximation to the diffusion process and insufficient spatial resolution.

There are two basic approaches in utilizing the information DTI data provides: Fiber tractography and connectivity mapping. The former attempts to answer the following question: Can we reconstruct the fiber that passes through a given seed point? Among different approaches, the Runge-Kutta method has been widely accepted [1]. However, fiber tracking is prone to cumulative errors and can not overcome the partial volume effect [2, 3]. In addition to that, the majority of tracking algorithms are based on estimating the underlying fiber's orientation. This is contrary to the nature of the DTI data, which provides an approximation to the diffusion process, thus it does not provide such an exact image of the structures. The second group of approaches attempts to utilize this nature of the DTI data by estimating a connectivity map. They consider each and every connection possibility but weight them as dictated by the DTI data.

Koch et al. used a Monte-Carlo simulation of the random walk model [4], Hangmann et al. extended this method by incorporating the white matter fiber tract curvature [5]. Chung et al. applied anisotropic Gaussian filtering of the transition probabilities of the underlying diffusion process [6]. Batchelor et al. solved the anisotropic diffusion equation set by the DTI data with the initial conditions being a set of seed points set to an initial nonzero concentration (of virtual diffusing particles) [7]. Lenglet et al., on the other hand, recasted the connectivity problem to Reimannian differential geometry framework where they defined their local metric tensor using the DTI data and solved for geodesics [8].

In this work, we propose a model based on a physical setup of nodes (no masses) and springs (whose spring constants were set according to the DTI data). We showed that the connectivity map associated to this physical system can be achieved by minimizing its total potential energy. The variational approach for computing this stationary pattern, has been found to be equivalent to a modified diffusion process. We showed that our method provides connectivity maps that correlate with normal anatomy on real patient data. The proposed method is fast to compute, has a tuning parameter that allows one to adjust the relative importance of the principal diffusion direction among other diffusion directions, allows multiple seed selection to incorporate a-priori information about the anatomy.

2 Method

In general, connectivity can be interpreted as a measure which is proportional to the qualitative similarity and spatial proximity of the units contained in data to be analyzed. In the case of DT images, where we are trying to reveal a functional connectivity, qualitative assessment of tensors becomes crucial in order to construct an appropriate model. We have to consider some certain features embedded in a DT image as indicators of connectivity. In general, the connectivity measure between two tensors can be visualized in terms of the volume overlap of their ellipsoids centered at the corresponding voxel coordinates. This interpretation will take the relative features of tensors into consideration such as their respective locations, sizes, orientations and shapes. A similar but simpler metric, that we proposed and used in this study is the so-called distance scaled mutual diffusion coefficient K. Given two tensors $\mathbf{D}_1$ and $\mathbf{D}_2$, located at $\mathbf{r}_1$ and $\mathbf{r}_2$, respectively, we define their connectivity K_{12} as:

$$K_{12} = \frac{[(\mathbf{v}^T\mathbf{D}_1\mathbf{v})(\mathbf{v}^T\mathbf{D}_2\mathbf{v})]^\gamma}{\delta^2} \tag{1}$$

where $\mathbf{v} = (\mathbf{r}_1 - \mathbf{r}_2)/\delta$ and $\delta = \|\mathbf{r}_1 - \mathbf{r}_2\|_2$. Thus, K reflects the mutual influence of tensor pairs by giving the distance scaled product of their diffusion coefficients evaluated in the unit direction of their Euclidean link and raised to the power γ, which will be used as a tuning parameter. For the time being we take γ to be 1. We can construct a physical system, based on K_{ij}'s which reflect the connectivity pattern within DTI data.

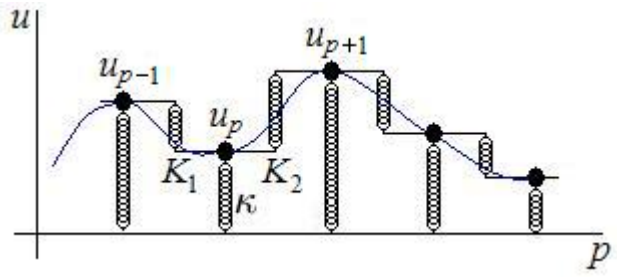

Fig. 1. Illustration of proposed spring system for a 1D curve (solid line), dots represent the nodes, spring constants are given for the specific node u_p.

Let $\Omega = [0, a] \times [0, b] \times [0, c] \subseteq \Re^3$ be our image domain, and let $\mathbf{D} : \Omega \rightarrow \Re^3 \times \Re^3$ be the given tensor field. We propose that the sought connectivity map $u : \Omega \rightarrow \Re$ with respect to a given seed point $(x_0, y_0, z_0) \in \Omega$ is the stationary pattern of a physical spring system defined as follows: Each voxel of the domain corresponds to a node and connectivity at seed node $u(x_0, y_0, z_0)$ is set to 1, which is kept constant in time. For each pair of adjacent nodes, a spring is associated with a stiffness, that is set to the mutual diffusion coefficient of Equation 1, evaluated for the adjacency of that particular pair. Thus, if we consider 6-neighborhood (N_6) on a regular 3D grid with δ-spacing in all directions, this model will correspond to 6 "neighbor springs" acting on each node and a node at $\mathbf{r}_i = (x, y, z)^T$ would share the following spring constant with respect to its immediate neighbor $\mathbf{r}_j = (x - \delta, y, z)^T$:

$$K_1(x, y, z) = \frac{(\mathbf{e}_1^T \mathbf{D}(x, y, z)\mathbf{e}_1)(\mathbf{e}_1^T \mathbf{D}(x - \delta, y, z)\mathbf{e}_1)}{\delta^2} \tag{2}$$

where $\mathbf{e}_1 = (1, 0, 0)^T // (\mathbf{r}_i - \mathbf{r}_j)$ is the unit vector of the orthonormal basis. Remaining constants of neighbor springs $K_2, ..., K_6$ are defined similarly with $\mathbf{e}_2 = (0, 1, 0)^T$ and $\mathbf{e}_3 = (0, 0, 1)^T$. We set their elongations as the local directional differences of u (for instance as $u(x, y, z) - u(x - \delta, y, z)$ for K_1), such that they force u to be equal to the corresponding immediate neighbor. Finally, an extra spring the so-called "ground spring" with a constant stiffness κ is also attached to all nodes, this time with the elongation u, forcing it to be 0. This is necessary to justify our model for revealing connectivity, which will be explained next. The resulting spring system can be visualized in Figure 1 for a 1D curve. With this model, total potential energy stored at these 7 springs will be given as:

$$V_{springs} = \frac{1}{2}\kappa u^2 + \sum_{n=1}^{6} V_n \tag{3}$$

where $V_1 = \frac{1}{2}K_1[u(x, y, z) - u(x - \delta, y, z)]^2$ and $V_2, ...V_6$ are defined similarly. In order to associate this potential energy to the point (x, y, z) rather than to

the springs, the latter six energy terms due to the neighbor connections should further be halved, as if they are equally shared with the corresponding neighbor. Otherwise they will be counted twice in the total energy summation of the map. We can also let $\delta \to 0$ assuming that we have infinite resolution, such that V can be approximated to a continuous function, enabling us to interpret the system better. Inserting K_n's common denominator δ^2 into the squared elongation terms and taking the limit, we obtain:

$$V(u, u_x, u_y, u_z) = \frac{1}{2}(\kappa u^2 + d_{11}^2 u_x^2 + d_{22}^2 u_y^2 + d_{33}^2 u_z^2) \tag{4}$$

where d_{jj} $(j = 1, 2, 3)$ are the diagonal elements of $\mathbf{D}$ as can easily be derived from Equation 2. We can put the current problem into a variational one, where the connectivity map u with respect to the seed at (x_0, y_0, z_0) can be found by minimizing the following energy functional:

$$J(u) = \int_\Omega V(u, u_x, u_y, u_z) d\Omega \tag{5}$$

assuming Neumann boundary conditions on $\partial\Omega$, and an extra seed condition $u(x_0, y_0, z_0) = 1$. Corresponding Euler-Lagrange equation is:

$$\kappa u - \frac{d}{dx}(d_{11}^2 u_x) - \frac{d}{dy}(d_{22}^2 u_y) - \frac{d}{dz}(d_{33}^2 u_z) = 0 \tag{6}$$

It is easy to show that fixing $u(x_0, y_0, z_0)$ to 1 for an interior point of Ω, does not change the Euler-Lagrange equation since $J(u)$ can be rewritten as a sum of several integrals evaluated at Cartesian subregions, each having (x_0, y_0, z_0) at their boundaries and sharing the same integrand. The physical interpretation of our model is as follows: A connected spring system, which is only lifted at (x_0, y_0, z_0) to a constant level of 1 and kept there, achieves its stationary pattern by minimizing its total potential energy. Nodes other than the seed try to come to zero due to the ground springs, but they will be lifted up as well, in proportion to their connectivity to the seed node, which remains at 1. Hence, the stationary pattern will be equivalent to the sought connectivity map with respect to the seed node.

Temporally evolving a given initial u_0 at a rate determined by the negative of the left term of Equation 6, by a steepest descent scheme, we obtain the following PDE:

$$u_t = -\kappa u + \frac{d}{dx}(d_{11}^2 u_x) + \frac{d}{dy}(d_{22}^2 u_y) + \frac{d}{dz}(d_{33}^2 u_z) = -\kappa u + \nabla \bullet (\widetilde{\mathbf{D}} \nabla u) \tag{7}$$

where $\widetilde{\mathbf{D}}$ is a diagonal matrix with squared diagonal entries of $\mathbf{D}$. The same equation could be obtained with another $\widetilde{\mathbf{D}}$, using different neighborhood (and/or spring) definitions. In any case, resulting PDE can be considered as a modified diffusion process, with a seed condition $u(x_0, y_0, z_0) = 1$ and an extra term $-\kappa u$, keeping u attached to the ground. Thus, as $t \to \infty$, u does not get totally flat,

although $\widetilde{\mathbf{D}}$, which is constant in time, governs the diffusion part. If we interpret the model in 2D, a structure sensitive tent-like pattern will be obtained with its stem being at the seed.

Numerical implementation of such a map evolution scheme can easily be accomplished by anisotropic diffusion filters with the specified modifications and an initial map:

$$u_0(x,y,z) = \begin{cases} 1 & if\ (x,y,z) = (x_0,y_0,z_0) \\ 0 & otherwise \end{cases} \tag{8}$$

Note that, we have started with a discrete model composed of finite number of nodes and springs, approximated it to a continuous case, derived the Euler-Lagrange equation and ended up with a meaningful PDE. Instead of reformulating and applying this PDE back to the discrete data, we prefer to keep our model in its discrete form since the beginning and consider the following functional as the summation version of Equation 5:

$$J(u) = \sum_p \{\kappa u_p^2 + \frac{1}{2}\sum_{n=1}^{N} K_{pn}(u_p - u_{pn})^2\} \tag{9}$$

where p is the voxel index and N is the number of neighbors. u_{pn} and K_{pn} stand for the n^{th} neighbor of the p^{th} node and its associated spring constant, respectively. $\frac{1}{2}$ scales the potential energy of neighbor springs, since they are counted twice in the outer summation. Now, writing the discrete Euler-Lagrange equation of this functional, i.e. assuming that u is an extremal, perturbing it with some $\epsilon\eta$, where η is also an arbitrary discrete map, and equating the derivative of perturbed functional with respect to ϵ (evaluated at $\epsilon = 0$) to zero we obtain:

$$\kappa u_p + \sum_{n=1}^{N} K_{pn}(u_p - u_{pn}) = 0 \tag{10}$$

Note that this equation says that along an extremal, the total spring force applied to each node is zero. This could also be observed by rewriting Equation 6 in a discrete form where space derivatives are replaced with central differences.

Seeking for the connectivity as a PDE evolution with diffusion filters, will bring the common trade-off between conservation of stability and rate of convergence, which actually is determined by an appropriate choice of the time step Δt. Thus we propose, another map evolution technique, which mimics the diffusion process in the light of the balanced force condition imposed by discrete Euler-Lagrange equation. Briefly, we say that, instead of calculating the update u_t, we can iteratively solve for a new u_p, which makes u_t vanish at p. "Balance in the neighborhood" condition dictated by Equation 10, locally and explicitly gives:

$$u_p = \frac{\sum_n^N K_{pn} u_{pn}}{\kappa + \sum_n^N K_{pn}} \tag{11}$$

This scheme with $\kappa = 0$ would be the same as assigning a weighted neighborhood average to each u_p, but with a spatially varying kernel coming from the local image structure. In fact, this adaptive directional smoothing constitutes the essence of the diffusion filtering, hence it can be interpreted to be equivalent to the diffusion process [6]. Equation 11 has a similar computational cost to Equation 7, but a higher convergence rate. Moreover, stability is naturally provided by the bounds specified by local neighborhood of u_{pn}'s.

In order to validate the computed connectivity maps, we used a simple tracking module, that follows coherence directions in converged u. As in [9], we first compute the structure tensor of u, which is obtained by taking the tensor product of its gradient and componentwise smoothing the resulting matrix:

$$\mathbf{S}(u) = G_\sigma * (\nabla u \otimes \nabla u) = \begin{bmatrix} \omega_1 & \omega_2 & \omega_3 \end{bmatrix} \begin{bmatrix} \lambda_1 & 0 & 0 \\ 0 & \lambda_2 & 0 \\ 0 & 0 & \lambda_3 \end{bmatrix} \begin{bmatrix} \omega_1^T \\ \omega_2^T \\ \omega_3^T \end{bmatrix} \tag{12}$$

where G_σ is a Gaussian kernel with variance σ^2. $\mathbf{S}(u)$ is a symmetric positive semidefinite matrix, which is invariant under sign changes of the gradient. Its magnitude ordered eigenvalues $\lambda_1 \geq \lambda_2 \geq \lambda_3$ give the amount of u's fluctuation, along the corresponding eigenvectors. Thus, as ω_1 will be parallel to the smoothed gradient, the smallest eigenvector ω_3, which is also called the coherent direction, will correspond to the orientation with least decrease in the connectivity. Starting from the seed, we can easily follow ω_3 vectors for tracking the candidate fiber.

3 Results

We used real patient data in our experiments to show that the computed connectivity maps agree with the known anatomy of the human brain. The scans were single-shot EPI scans with diffusion encoding along 12 non-collinear directions plus one reference without diffusion-weighting. The FOV was 25-26cm, TE was minimum with partial k-space acquisition. TR was $\sim 10s$ and b-value was $\sim 850s/mm^2$.

Experiments are comparatively conducted based on 26 neighborhood for different seed points. Note that, with N_{26}, spring constants for corners of a $3\times3\times3$ neighborhood cube, appear with weights $\frac{1}{2}$ and $\frac{1}{3}$ due to the denominator δ^2. Stiffness for the ground springs is empirically taken to be $\frac{1}{100}$ of the mean neighbor stiffness of the whole domain and converged maps are visualized in the log-scale. Convergence of the iterations was assumed when the mean absolute change in u dropped below 10^{-4} with $u \in [0, 1]$. Qualitative evaluation of the results were done based on the computed connectivity maps and the tracts computed from u maps.

Figure 2 shows axial cross-sections of the computed 3D connectivity maps with different γ values, ranging from 2 to 10. Note the correlation between the connectivity map and the brain anatomy as well as the assigned connectivity values with respect to the seed point. The anatomy is enhanced as γ increases.

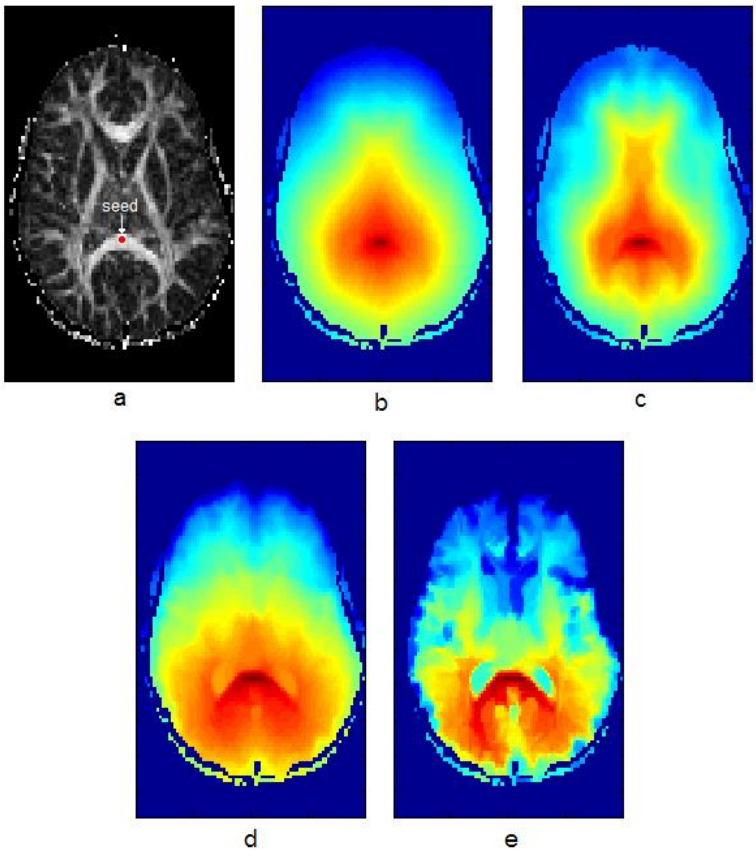

Fig. 2. a) Axial slice of FA map with the seed indicated, b) Converged connectivity map ($\gamma = 1$, red corresponds to high connectivity), c-e) Converged maps for $\gamma = 2, 4, 10$,

Figure 3 shows connectivity surface with $\gamma = 10$ at the axial slice with its coherent directions and tracts computed by following these vectors as defined in [9]. They also correlate with the underlying fiber structure.

The overall computation in a $128 \times 128 \times 38$ volume lasted for less than 100 seconds with Matlab R14 using a PC with P4 2.4 GHz processor and 2GB RAM.

4 Discussion

In this study we proposed a novel method for computing the connectivity in white matter. We associated the DT-image to a physical spring system, and interpreted the underlying connectivity to be its stationary pattern. We followed a variational approach, which aims to minimize the total spring potential energy and showed that, the PDE evolution scheme coming from the Euler-Lagrange

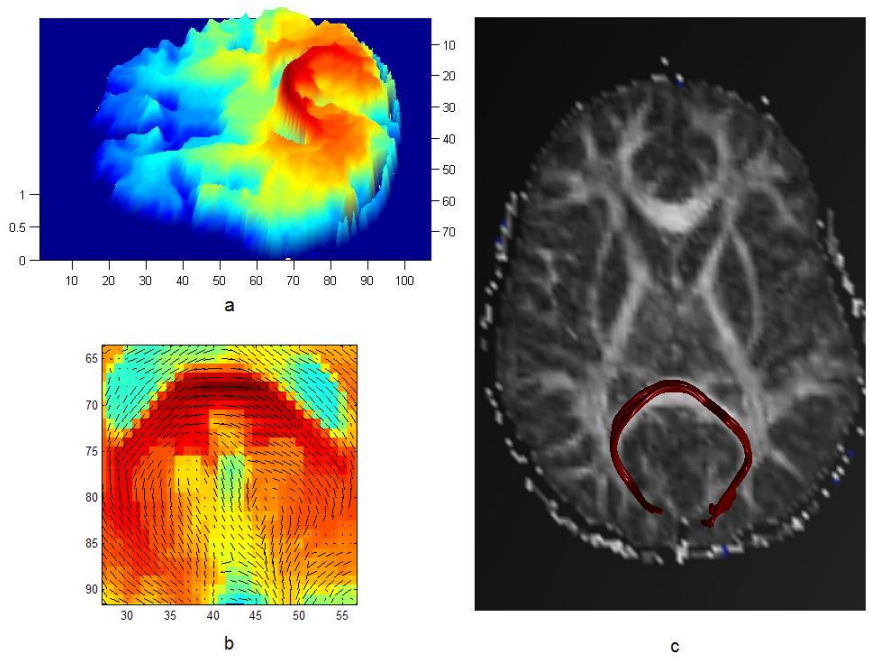

Fig. 3. a) Connectivity surface for axial slice with $\gamma = 10$, b) Coherent vectors on connectivity map, c) Computed tracts, by following coherent vectors

equation corresponds to a modified diffusion process. Reformulating the energy minimization problem in the discrete domain enabled us to replace the PDE with an alternative directional averaging method, which guarantees stability and exhibits a higher convergence rate.

The proposed method is computationally inexpensive and provides several advantages. It is flexible for different definitions of neighborhood and spring constants, still preserving the same physical model. Thus we use a tuning parameter γ that allows one to continuously trade-off using the complete DTI data with getting enhanced anatomical information based on the principal diffusion direction only. At one end, our method corresponds to the tractography approach (large γ) and at the other hand it corresponds to complete connectivity model ($\gamma = 1$).

Another advantage is that it allows to set multiple seed points, even regions. Thus, one can easily incorporate a-priori information about the anatomy into the connectivity map computation, by selecting seeds which are known in advance to be connected. The computational cost is independent of the number of selected seed points.

As mentioned above ground springs are necessary for preventing total flattening of u, such that we obtain meaningful maps that monotonically decrease as we get away from the seed. The stiffness κ of the ground springs does not make much difference as long as it is nonzero. κ should be sufficiently small, such that the farthest point of the brain can also attain a nonzero connectivity value and should be large enough so that the converged map does not become nearly flat. We empirically set it to be $\frac{1}{100}$ of the mean of neighbor spring constants.

5 Appendix

A. Derivation of Euler-Lagrange equation from the sum functional: Writing Equation 9 explicitly, as a summation over discrete 3D grid indices $p = (i, j, k)$ and for N_6, we obtain:

$$\begin{aligned} J(u) = \sum_{i,j,k} \big\{ & \kappa u^2(i,j,k) \\ & + \frac{1}{2} K_1(i,j,k)[u(i,j,k) - u(i-1,j,k)]^2 \\ & + \frac{1}{2} K_2(i,j,k)[u(i,j,k) - u(i+1,j,k)]^2 \\ & + \frac{1}{2} K_3(i,j,k)[u(i,j,k) - u(i,j-1,k)]^2 \\ & + \frac{1}{2} K_4(i,j,k)[u(i,j,k) - u(i,j+1,k)]^2 \\ & + \frac{1}{2} K_5(i,j,k)[u(i,j,k) - u(i,j,k-1)]^2 \\ & + \frac{1}{2} K_6(i,j,k)[u(i,j,k) - u(i,j,k+1)]^2 \big\} \end{aligned}$$

Due to symmetry in neighbor springs, we have $K_1(i,j,k) = K_2(i-1,j,k)$, $K_3(i,j,k) = K_4(i,j-1,k)$ and $K_5(i,j,k) = K_6(i,j,k-1)$. Thus, terms involving K_2, K_4 and K_6, will reappear with odd subscripts at the next summand of corresponding summing dimension. So we drop $\frac{1}{2}$'s and rewrite the summation for preceding neighbors, only:

$$\begin{aligned} J(u) = \sum_{i,j,k} \big\{ & \kappa u^2(i,j,k) \\ & + K_1(i,j,k)[u(i,j,k) - u(i-1,j,k)]^2 \\ & + K_3(i,j,k)[u(i,j,k) - u(i,j-1,k)]^2 \\ & + K_5(i,j,k)[u(i,j,k) - u(i,j,k-1)]^2 \big\} \end{aligned}$$

Let u be an extremal for J, and let η be an arbitrary perturbation function defined on the same discrete domain. For the perturbed connectivity $\widetilde{u} = u + \epsilon\eta$ with small ϵ to be a valid map, η must be zero on the seed. Furthermore, it is zero on the boundary, too which is practically the case for u as well, since **D**

is nonzero within some interior subvolume of Ω, corresponding to the cortex. Writing the functional for the perturbed map we have:

$$\begin{aligned}J(\widetilde{u}) = \sum_{i,j,k} \big\{ & \kappa[u(i,j,k) + \epsilon\eta(i,j,k)]^2 \\ & + K_1(i,j,k)[u(i,j,k) + \epsilon\eta(i,j,k) - u(i-1,j,k) - \epsilon\eta(i-1,j,k)]^2 \\ & + K_3(i,j,k)[u(i,j,k) + \epsilon\eta(i,j,k) - u(i,j-1,k) - \epsilon\eta(i,j-1,k)]^2 \\ & + K_5(i,j,k)[u(i,j,k) + \epsilon\eta(i,j,k) - u(i,j,k-1) - \epsilon\eta(i,j,k-1)]^2 \big\}\end{aligned}$$

Now, since u is an extremal, for all η satisfying aforementioned conditions, we must have:

$$\begin{aligned}& \left.\frac{\partial J(\widetilde{u})}{\partial \epsilon}\right|_{\epsilon=0} = 0 \\ &= \sum_{i,j,k} \kappa u(i,j,k)\eta(i,j,k) \\ &+ \sum_{j,k}\left\{\sum_i K_1(i,j,k)[u(i,j,k) - u(i-1,j,k)][\eta(i,j,k) - \eta(i-1,j,k)]\right\} \\ &+ \sum_{i,k}\left\{\sum_j K_3(i,j,k)[u(i,j,k) - u(i,j-1,k)][\eta(i,j,k) - \eta(i,j-1,k)]\right\} \\ &+ \sum_{i,j}\left\{\sum_k K_5(i,j,k)[u(i,j,k) - u(i,j,k-1)][\eta(i,j,k) - \eta(i,j,k-1)]\right\} \quad (13)\end{aligned}$$

where for the latter three energy terms, we changed the order of summations according to the direction of differences they contain. Note that each summand of these inner summations will share terms involving $\eta(i,j,k)$ with its successor. Collecting these, we can rewrite Equation 13 as:

$$\begin{aligned}0 = & \sum_{i,j,k} \kappa u(i,j,k)\eta(i,j,k) \\ & + \sum_{j,k}\left\{\sum_i \eta(i,j,k)\big\{K_1(i,j,k)[u(i,j,k) - u(i-1,j,k)]\right. \\ & \left. + K_1(i+1,j,k)[u(i,j,k) - u(i+1,j,k)]\big\}\right\} \\ & + \sum_{i,k}\left\{\sum_j \eta(i,j,k)\big\{K_3(i,j,k)[u(i,j,k) - u(i,j-1,k)]\right. \\ & \left. + K_3(i,j+1,k)[u(i,j,k) - u(i,j+1,k)]\big\}\right\} \\ & + \sum_{i,j}\left\{\sum_k \eta(i,j,k)\big\{K_5(i,j,k)[u(i,j,k) - u(i,j,k-1)]\right. \\ & \left. + K_5(i,j,k+1)[u(i,j,k) - u(i,j,k+1)]\big\}\right\}\end{aligned}$$

$$+\sum_{j,k}\eta(1,j,k)[u(1,j,k)-u(2,j,k)]+\eta(X,j,k)[u(X,j,k)-u(X-1,j,k)]$$
$$+\sum_{i,k}\eta(i,1,k)[u(i,1,k)-u(i,2,k)]+\eta(i,Y,k)[u(i,Y,k)-u(i,Y-1,k)]$$
$$+\sum_{i,j}\eta(i,j,1)[u(i,j,1)-u(i,j,2)]+\eta(i,j,Z)[u(i,j,Z)-u(i,j,Z-1)]$$

where $(1...X, 1...Y, 1...Z)$ is the size of the grid. What is done here is analogous to integration by parts. Last three terms are evaluated at the bounding planes of Ω, so they are zero. Again due to the symmetry of neighbor springs, we can replace $K_1(i+1,j,k)$, $K_3(i,j+1,k)$ and $K_5(i,j,k+1)$ with $K_2(i,j,k)$, $K_4(i,j,k)$ and $K_6(i,j,k)$, respectively. Thus we end up with:

$$\begin{aligned}0=&\sum_{i,j,k}\eta(i,j,k)\big\{\kappa u(i,j,k)\\&+K_1(i,j,k)[u(i,j,k)-u(i-1,j,k)]\\&+K_2(i,j,k)[u(i,j,k)-u(i+1,j,k)]\\&+K_3(i,j,k)[u(i,j,k)-u(i,j-1,k)]\\&+K_4(i,j,k)[u(i,j,k)-u(i,j+1,k)]\\&+K_5(i,j,k)[u(i,j,k)-u(i,j,k-1)]\\&+K_6(i,j,k)[u(i,j,k)-u(i,j,k+1)]\big\}\\=&\sum_p\eta_p\bigg\{\kappa u_p+\sum_{n=1}^{6}K_{pn}(u_p-u_{pn})\bigg\}\end{aligned}\tag{14}$$

Lemma: For Equation 14 to hold for all valid η, i.e. for u to be an extremal, $\kappa u_p+\sum_n K_{pn}(u_p-u_{pn})$ must be identically zero for all $p\in\Omega$.
Proof: Assume that $\kappa u_p+\sum_n K_{pn}(u_p-u_{pn})$ is nonzero for some p^*. Then, there exists a valid η, such that it is also nonzero at p^*, but everywhere else. Thus, the summation becomes nonzero, which contradicts with Equation 13. Hence, we obtain the Euler-Lagrange equation as $\kappa u_p+\sum_n K_{pn}(u_p-u_{pn})=0$.

B. Experimental Justification of Equivalence between Diffusion Filtering and Adaptive Kernel Smoothing:
Let us first consider Perona-Malik diffusion filter for regularizing an image given as $u:\Omega=[0,a]\times[0,b]\subseteq\Re^2\rightarrow[0,255]\subseteq\Re$ with the following PDE:

$$\frac{\partial u}{\partial t}=\nabla\bullet\big(g(\|\nabla u\|)\nabla u\big)=\frac{d}{dx}\big(g(\|\nabla u\|)u_x\big)+\frac{d}{dx}\big(g(\|\nabla u\|)u_y\big)\tag{15}$$

where diffusivity is given as:

$$g(\|\nabla u\|)=exp\bigg\{-\frac{\|\nabla u\|^2}{\sigma^2}\bigg\}=exp\bigg\{-\frac{u_x^2+u_y^2}{\sigma^2}\bigg\}\tag{16}$$

The right hand side of Equation 15 comes from the following functional:

$$J(u) = \int_{\Omega} \frac{\sigma^2}{2} exp\left\{ -\frac{u_x^2 + u_y^2}{\sigma^2} \right\} d\Omega \tag{17}$$

with the Euler-Lagrange equation to be satisfied along any extremal:

$$\frac{d}{dx}\big(g(\|\nabla u\|)u_x\big) + \frac{d}{dx}\big(g(\|\nabla u\|)u_y\big) = 0 \tag{18}$$

Hence, given an initial image u_0, the diffusion process actually maximizes J by temporally updating the image, with the amount given by the left hand side of Equation 18. With the same goal of reaching an extremal, that satisfies this equation (i.e. that achieves a state of the diffusion process, for which $u_t = 0$ for all $x, y \in \Omega$), we can alternatively let the image evolve to the converged result by locally solving for u that satisfies the Euler-Lagrange equation, i.e. that makes u_t locally vanish.

As it is in our case, let us consider Equation 18 in the discrete sense, which can also be derived from a summation functional(see Appendix-A):

$$\begin{aligned} 0 = & \frac{g(i+1,j)\frac{u(i+2,j)-u(i,j)}{2} - g(i-1,j)\frac{u(i,j)-u(i-2,j)}{2}}{2} \\ & + \frac{g(i,j+1)\frac{u(i,j+2)-u(i,j)}{2} - g(i,j-1)\frac{u(i,j)-u(i,j-2)}{2}}{2} \end{aligned} \tag{19}$$

where local diffusivity is written as $g(i,j) = g(\|\nabla u\|)\big|_{i,j}$ and derivatives are replaced by central differences. Simplifying Equation 19 we obtain:

$$\begin{aligned} 0 = & \, g(i+1,j)[u(i,j) - u(i+2,j)] + g(i-1,j)[u(i,j) - u(i-2,j)] \\ & + g(i,j+1)[u(i,j) - u(i,j+2)] + g(i,j-1)[u(i,j) - u(i,j-2)] \end{aligned} \tag{20}$$

As in the proposed physical model, Euler Lagrange equation in this form, can be thought as the force equation of a spring system, where for each node (i,j), there are four springs with constants $g(i+1,j)$, $g(i-1,j)$, $g(i,j+1)$ and $g(i,j-1)$ as functions of local structure, and with respective elongations $[u(i,j) - u(i+2,j)]$, $[u(i,j) - u(i-2,j)]$, $[u(i,j) - u(i,j+2)]$ and $[u(i,j) - u(i,j-2)]$. With this analogy, the springs can be thought as the image-flattening units trying to pull the image intensity to the levels of its neighbors. Thus we can replace the PDE-evolution of the diffusion filter with an iterative and adaptive kernel smoothing method by locally solving Equation 20 for u, at each pixel $p = (i,j)$:

$$u_p = \frac{\sum_n^4 g_{pn} u_{pn}}{\sum_n^4 g_{pn}} \tag{21}$$

where subscript pn stands for the n^{th} neighbor of the p^{th} pixel. Compared to PDE-scheme, which is sensitive to the time step as in the numerical applications of diffusion filtering, Equation 21 has a higher convergence rate, requiring the

Fig. 4. Top-Left: Original 'cameraman' image, Top-Right: Its noisy version with noise standard deviation 20, Bottom-Left: Regularization with adaptive kernel smoothing formulated from Perona-Malik diffusion, Bottom-Right: Regularization with adaptive kernel smoothing formulated from edge-enhancing diffusion

same amount of flops per iteration. Moreover, stability is naturally guaranteed by the bounds specified by local neighborhood.

The same approach can be extended to other anisotropic tensor diffusion schemes, by defining the weights, i.e. the spring constants as functions of diffusion tensor's components. Figure 4 shows examples of regularizing a 256×256 noisy image with adaptive kernel smoothing methods, which are formulated equivalent to Perona-Malik and edge enhancing diffusion filters. Convergence criterion is the mean absolute change in $u \in [0, 255]$, falling below some threshold, which is taken to be 1. Input noise standard deviation is 20. The process converges to the regularized results in 4-5 iterations and in less than 0.5 seconds with Matlab R14 using a PC with P4 2.4 GHz processor and 2GB RAM.

References

1. Tench, C.R., Morgan, P.S., Wilson, M., Blumhardt, L.D.: White Matter Mapping Using Diffusion Tensor MRI. Magn. Res. Med. 47 (2002) 967972

2. Alexander, A.L., Hasan, H.M., Lazar, M., Tsuruda, J.S., Parker, D.L.: Analysis of Partial Volume Effects in Diffusion-Tensor MRI. Magn. Res. Med. 45 (2001) 770-780.

3. Basser, P.J., Pajevic, S., Pierpaoli, C., Duda, J., Aldroubi, A.: In vivo tractography using DT-MRI data. Magn. Res. Med. 44 (2000) 625-632

4. Koch, M.A., Norris, D.G., and Hund-Georgiadis, M.: An Investigation of Functional and Anatomical Connectivity using Magnetic Resonance Imaging. NeuroImage 16 (2002) 241-250.

5. Hagmann, P., Thiran, J.-P., Vandergheynst, P., Clarke, S., Meuli, R.: Statistical Fiber Tracking on DT-MRI Data as a Potential Tool for Morphological Brain Studies. ISMRM Workshop on Diffusion MRI: Biophysical Issues (2000).

6. Chung, M.K., Lazar, M., Alexender, A.L., Lu, Y., Davidson, R.: Probabilistic Connectivity Measure in Diffusion Tensor Imaging via Anisotropic Kernel Smoothing. University of Wisconsin, Dept. of Statistics (2003) Technical report no: 1081

7. Batchelor, P.G., Hill, D.L.G., Atkinson, D., Calamanten, F., Atkinson, D.: Study of Connectivity in the Brain using the Full Diffusion Tensor from MRI. IPMI 2001, Lecture Notes in Computer Science 2082 (2001) 121-133.

8. Lenglet, C., Deriche, R., Faugeras, O.: Diffusion Tensor Magnetic Resonance Imaging: Brain Connectivity Mapping. INRIA (2003) Technical report no: 4983

9. Weickert, J.: Coherence-Enhancing Diffusion Filtering. International Journal of Computer Vision 31(2/3) (1999) 111127

10. Perona, P., Malik, J.: Scale Space and Edge Detection using Anisotropic Diffusion. IEEE Trans. on Pattern Analysis and Machine Intelligence, Vol. 12 , No. 7, (1990) 629 - 639.

11. van Brunt, B.: The Calculus of Variations. Springer-Verlag New York, Inc (2004)